Simulation of the effect of atmospheric stratification on the power production of a wind farm

Bachelor Thesis

K. Steinebach

Delft University of Technology

TU Delft Delft University of Technology

Challenge the future

SIMULATION OF THE EFFECT OF ATMOSPHERIC STRATIFICATION ON THE POWER PRODUCTION OF A WIND FARM

BACHELOR THESIS

by

K. Steinebach

To obtain the degree of Bachelor of Science in 'Applied Physics' at the Faculty of Applied Sciences at the Delft University of Technology, to be defended privately on Thursday August 24, 2017 at 4:00 PM.

Bachelor of Science
in Applied Physics

Under supervision of the Atmospheric Physics group
Department of Geoscience and Remote Sensing
Faculty of Civil Engineering
Delft University of Technology

Student number:	4372549
Project duration:	April 24, 2017 – August 24, 2017
Supervisor:	Dr. S. R. de Roode
Thesis committee:	Dr. S. R. de Roode
	Prof. dr. A. P. Siebesma

TU Delft Delft University of Technology

ABSTRACT

The wind energy industry is growing more than ever before and wind energy as a renewable energy source has shown quite a potential over the years. Unfortunately, the power yield of a wind farm can fluctuate largely over time, which originates from fluctuating wind speed magnitudes. Convection of air, turbulence, humidity and radiation of heat are processes in the atmospheric boundary layer, the lowest region of the troposphere above Earth's surface, that are responsible for these fluctuations. This region is characterized by a diurnal cycle in which two examinable cases can be found, namely the convective boundary layer (CBL) case during the daytime period and the stable boundary layer (SBL) case during the nighttime period of the diurnal cycle. In the SBL case, the earlier mentioned physical processes result in a cool surface layer and relatively little turbulence is present, whereas in the CBL case a relatively warm surface layer and high turbulence level are present. The Dutch Atmospheric Large Eddy Simulation (DALES) model is used in which wind turbines are implemented with the help of former TU Delft master student P.A. van Dorp. With DALES, a simulation is performed for each case and the output data of the two simulations are analysed and compared to find the optimal case in terms of total power yield of a configuration of two wind turbines with the second fully in the wake produced by the one in front. An arbitrary distance of 600m between the wind turbines is chosen, which corresponds to 7.5 times the diameter length of the wind turbines, and a hub height of 80m is chosen. First, the simulations are validated by examining the turbulent kinetic energy profiles. Then, the wind speed profiles over the domain are analysed, corresponding to the turbulent kinetic energy profiles and showing that the average wind speed at hub height for the SBL case is larger than for the CBL case. Furthermore, the wake profiles behind the turbines are displayed and compared for the two cases, showing little difference. Finally, the total power yield of this specific wind turbine configuration is calculated. With an average power yield of 1.71MW for the SBL case compared to 0.90MW for the CBL case, the SBL case is shown to be the optimal atmospheric boundary layer case in terms of power production for this specific wind turbine configuration.

CONTENTS

1

INTRODUCTION

1.1. WIND ENERGY

In the world of today, massive amounts of fossil fuel are consumed each day. Clearly, fossil fuel reserves are finite and from the amount of energy consumption in the past, it is calculated that the coal, gas and oil reserves together will be gone by the year of 2088 (Ecotricity, n.d.). Therefore, there is an urgent demand for other possible energy sources, and in particular renewable energy sources to foresee the need of energy in the future.

Wind energy is a possible renewable energy source for this problem. The wind energy industry is growing rapidly and has a high potential of increasing its market share in the energy market in the future. Wind is free to use and the amount of wind in nature is unlimited. This means that there is no exhaustion of energy sources in this field. Also, the production of energy from wind leads to a decrease in CO_2 emission compared to energy production from fossil fuel sources, which is positive for the environment (Awea, 2016). Extensive research has already been done in the field of wind energy, but more research is needed to overcome the high costs of wind farms and to achieve a higher cost efficiency from wind energy. The price of wind energy has already been decreasing rapidly over the last 20 years and the installed capacity of wind turbines has been increasing rapidly, however definitely more research is needed to compete with other energy sources of today like energy from fossil fuel, nuclear energy and solar energy (Latham, 2011).

One big disadvantage of wind energy is that there occur large fluctuations in wind speed and direction which make it difficult to predict the motion of wind over a long period of time. These fluctuations in wind speed and orientation result in large fluctuations in the power output of a wind farm, which is undesirable. A wind farm consists of a configuration of wind turbines in an array and in such a wind farm energy is generated by the process of extracting power (through kinetic energy) from the natural air flow. Therefore, the wind turbines in the front row of a wind farm disturb the natural flow of air behind the turbine. This results in a lower power production of the wind turbines on the next row. In a wind farm the wind turbines are conventionally placed a significant distance of about seven times the diameter length of a turbine apart. This distance is needed to obtain the conditions of the natural air flow back in front of the next row of turbines and to achieve the desired large power yield. However, a larger distance between the rows of wind turbines leads to higher costs for the area that the wind farm is built on and therefore, research has been done extensively in the past to determine the optimal balance between wind turbine distance and power production. Meyers and Meneveau (2012) for example found an average optimal distance of 15 times the rotor diameter which is considerably higher than the conventionally used distance. This optimal distance is very site dependent and has to be examined for each seperate wind farm, because at each site there are different average wind speeds and different probabilities that the wind is propagating in a certain direction. Also, the costs of land and sea areas differ largely. However, the theory of optimalization stays the same.

The power generated by a wind turbine is the result of extracting kinetic energy from the flowing wind. The power P that can be generated by a single wind turbine is proportional to the volumetric flow rate AU and the kinetic energy per unit volume of the wind $\frac{1}{2}\rho U^2$. In equation (1.1), the power production formula is shown.

$$P = \frac{1}{2}\rho C_p A U^3 \tag{1.1}$$

In equation (1.1) ρ is the density of air at hub height and C_P is a dimensionless proportionality constant with its maximum value equaling $C_{p,max} = \frac{16}{27}$ at optimal production level, which follows from Betz' limit. $A = \pi R^2$ is the area of the turbine rotor and U is the local wind speed at hub height in front of the turbine rotor. One important remark about this equation is that the power production of a wind turbine is proportional to the wind speed cubed, so a slight difference in wind speed has a large influence on the power yield. The area behind a turbine in which the flow of air is disturbed by power extraction is called a wake. In this wake the disturbed wind flow is slowly mixing with undisturbed wind near the wake and over distance the disturbed wind speed is increasing back towards the undisturbed wind speed value, U_∞. The distance that is needed to obtain the undisturbed wind speed value back is called the wake distance. In equation (1.2) below, the wind speed evolution over distance behind a turbine is shown compared to the undisturbed wind speed value (Boeker and van Grondelle, 2011).

$$\frac{U(x)}{U_\infty} = 1 - \frac{2a}{(1 + \frac{\alpha x}{\gamma R_T})^2} \tag{1.2}$$

In equation (1.2) x is the distance behind the turbine that created the wake, a is the induction factor of the turbine with an optimal value of $a = \frac{1}{3}$, α is an empirically determined value that accounts for the assumption that the shape of the wake profile is conical and with which constant, the atmospheric conditions are simplified and incorporated into the formula. γ is a factor that is only dependent on the induction factor of the turbine ($\gamma = \sqrt{\frac{1-a}{1-2a}}$) and R_T is the radius of the turbine rotor. In appendix 1, the derivation of this formula is given, which is a result from momentum theory and originates from the 'Jensen wake model'.

In the field of atmospheric science, it would be interesting to review how the behavior of wake recovery behind a wind turbine differs for different atmospheric conditions, in particular for different turbulence levels and surface heat fluxes. An accurate assessment of wind speeds throughout a wind farm is important to optimize the wind turbine configuration in that wind farm and thus maximize the produced power output. On the other hand, more accurate assessments on the power production level could give better insight in the fatigue load evolution on the turbines. This could in turn result in more accurate maintenance work and better cost efficiency.

1.2. ATMOSPHERIC STRATIFICATION

For this research, the physical processes that influence the power production of wind farms, which do conventionally have a maximum reached height of around 200m, are important and therefore the lowest atmospheric region above Earth's surface will be discussed, which is the troposphere. The troposphere has a height ranging between 7km and 20km at different latitudes and is divided into multiple layers. The lowest region of the troposphere will be discussed in which friction with Earth's surface influences the natural flow of air. This region is the planetary boundary layer or in literature also known as the atmospheric boundary layer (ABL) and has a height ranging between 50m during the night and 2km during the day. The atmospheric boundary layer is characterized by a diurnal cycle in which different net heat fluxes are present at Earth's surface. From this daily cycle, two cases will be examined on the difference in power production of a configuration of two wind turbines behind each other as a simplification of a large wind farm.

The first case is the convective boundary layer (CBL) case which arises during daytime and is driven by radiation from the sun heating up the surface of Earth. The net heat flux at Earth's surface is positive in this case, resulting in vertical air motions and turbulence with rapid fluctuations of wind speed and orientation. The other case is the stable boundary layer (SBL) case, which arises during nighttime when Earth is radiating more heat than it absorbs. Earth's surface is cooling down and relatively little turbulence in air is present. In the transition between the CBL case and the SBL case, there has to be the case in which the net surface heat flux is zero. This case is the neutral boundary layer (NBL) case. The NBL case however will not be examined as it can be seen as a transition case between the CBL case and the SBL case. In figure 1.1 below, the daily cycle of the atmospheric boundary layer is shown (Elte, 2011).

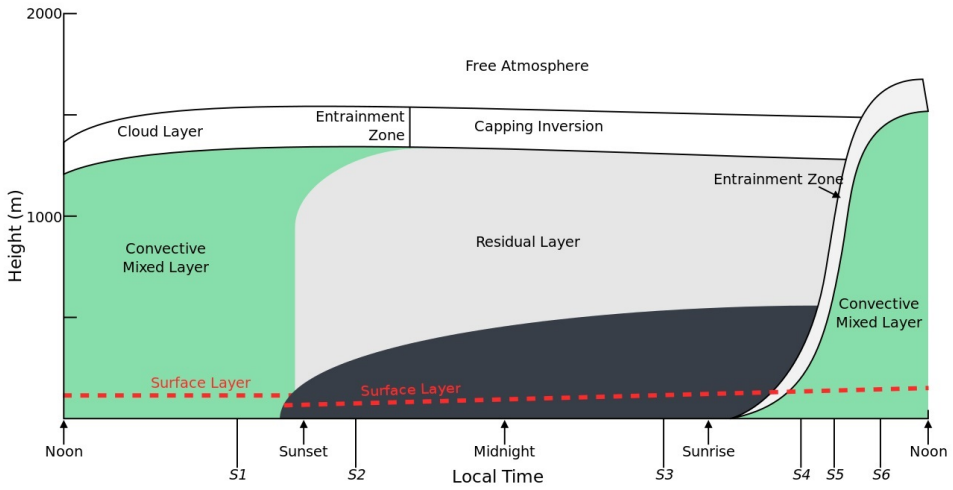

Figure 1.1. A daily cycle of the atmospheric boundary layer (Elte, 2011).

The first of the three important layers in the atmospheric boundary layer is the surface layer. This layer accounts for the lowest 10% of the atmospheric boundary layer and is characterized by a strong wind shear and friction with Earth's surface. The second of the three layers is called the mixed zone during daytime or the residual layer during nighttime. This layer is located between 10% and 80% of the atmospheric boundary layer and is during daytime characterized by a nearly constant potential temperature, wind speed and humidity profile over height because of strong buoyancy generating convective turbulent mixing (Piironen, 1996). The third and final layer is the capping inversion layer or also called the entrainment zone at daytime. This layer is located at the top 20% of the atmospheric boundary layer, is mostly characterized by thermal inversion and determines the height of the ABL. Thermal inversion means that temperature is increasing with height. On top of the ABL is the free atmosphere located. In the free atmosphere the wind is approximately geostrophic, which means that the wind is travelling parallel to the isobars. This is a characteristic meaning that friction with Earth's surface is not noticeably present anymore.

1.3. PROJECT OUTLINE

In this research, the 3D wind field in a domain containing a configuration of two wind turbines, with the second fully in the wake produced by the one in front, is simulated for the SBL case and the CBL case. To analyse the wake profiles, the power yield of this configuration and other parameters, the Dutch Atmospheric Large Eddy Simulation (DALES) model is used. DALES is a numerical turbulence simulation model widely used and verified by researchers from Delft University of Technology (TU Delft), Wageningen University (WUR), the Royal Dutch Meteorological Institute (KNMI) and the Max Planck Institute for Meteorology. In DALES a domain is specified for each simulation and initial and boundary conditions are specified in terms of the initial (geostrophic) wind speed and orientation and potential temperature profile or surface heat flux. The wind turbine implementation was performed by former TU Delft master student, P.A. van Dorp, who verified

and validated his model against power curves of two types of wind turbines and wind farm production data (van Dorp, 2016). With this extension of the DALES model, two Vestas V80 turbines are incorporated in the domain with an arbitrary distance of 600m between each other and their specifications are introduced as a rotor diameter of 80m and a hub height of 80m.

For the two cases the turbulent kinetic energy profiles will be examined for a verification of the simulations. With this verification in mind, the temporal and spatial evolution of the wind field will be visualized. This will give insight in which of the two cases the average wind speed at hub height is higher and for which case the wake behind the turbines is longer. Finally, the total power yield of this specific wind turbine configuration will be calculated to conclude on the optimal ABL case (SBL or CBL) in terms of power production.

In chapter 2, the experimental methodology of this study, the DALES model and the wind turbine implementation in DALES will be explained in more detail. The SBL case is taken from Beare et al (2006), and the CBL case is amongst other things adjusted with a prescribed surface heat flux. In chapter 3, the results of the simulations, which are needed to answer the research question, will be displayed and discussed. In chapter 4, the results and discussion points will be concluded and recommendations for future research will be proposed.

As a very short summary, the objective of this thesis would be: "Analysing and comparing the wind field and wake evolution in a domain with two wind turbines for two cases, CBL and SBL, to make a conclusion about the optimal atmospheric boundary layer case in terms of the total power yield in a configuration of two wind turbines with the second turbine fully in the wake produced by the one in front, an arbitrary distance of 600m apart."

2

EXPERIMENTAL METHODOLOGY FOR ABL STUDY

In this chapter, the DALES model, the wind turbine implementation in DALES and the experimental methodology of this study will be explained in more detail. Also, extensive details of the simulation of each case will be given with the SBL case taken from Beare et al (2006). Finally in this chapter, the methods of analysing output data from the simulations will be clarified.

2.1. DALES MODEL

The simulations, performed by DALES, belong to the field of computational fluid dynamics (CFD). The turbulent flow of air above the surface of Earth, convection of air and radiation of heat are processes that influence each other during such a simulation. To solve the dynamics between these processes, the equations for conservation of mass and momentum in the physics of turbulent flows, which are the continuity equation and the Navier-Stokes equation, need to be solved. In equation (2.1) and (2.2) respectively, the continuity equation and the Navier-Stokes equation in 3D are displayed (Multiphysics Cyclopedia, 2017).

$$\frac{\partial \rho}{\partial t} + \nabla \cdot (\rho \vec{\boldsymbol{U}}) = 0 \tag{2.1}$$

$$\rho(\frac{\partial \vec{\boldsymbol{U}}}{\partial t} + \vec{\boldsymbol{U}} \cdot \nabla \vec{\boldsymbol{U}}) = -\nabla p + \mu \nabla^2 \vec{\boldsymbol{U}} + \vec{F} \tag{2.2}$$

$\vec{\boldsymbol{U}} = (U, V, W)$ is the wind speed vector with U the wind speed component in the east-west direction, V the wind speed component in the north-south direction and W the vertical wind speed component, ρ is the density of the fluid, p the pressure, μ the dynamic viscosity and $\vec{F}$ the force that acts on a fluid. An exact solution to the Navier-Stokes equations is not present yet, therefore methods are needed to solve these equations numerically. The basic principle to perform calculations in CFD models is by dividing the domain in small control volumes and then solving the governing equations to each of these control volumes with certain initial conditions and boundary conditions. This is in short what DALES is programmed to execute, however DALES uses a simplified version of the two governing equations to solve the spatial and temporal evolution of the wind field, assuming that air is incompressible and thus has a constant density within a fluid parcel. This gives rise to equations (2.3) and (2.4) (Heus et al., 2010).

$$\nabla \cdot \vec{\boldsymbol{U}} = \frac{\partial U}{\partial x} + \frac{\partial V}{\partial y} + \frac{\partial W}{\partial z} = 0 \tag{2.3}$$

$$\frac{\partial \vec{\boldsymbol{U}}}{\partial t} = -\vec{\boldsymbol{U}} \cdot \nabla \vec{\boldsymbol{U}} + \frac{g}{\theta_0}\theta - \nabla \pi - \nabla \tau + \epsilon_{ij} f(\vec{\boldsymbol{U}} - \vec{\boldsymbol{U}}_{geo}) \tag{2.4}$$

In turbulent flows, the buoyancy forces caused by thermal fluctuations play an important role. The term $f(\vec{\boldsymbol{U}} - \vec{\boldsymbol{U}}_{geo})$ accounts for these buoyancy forces with the factor f accounting for the coriolis force which originates from Earth's rotation. $f = 2\Omega\sin(\phi)$ with Ω the angular velocity of Earth and ϕ the latitude on Earth. ϵ_{ij} is the Levi-Civita symbol which equals +1 when solving for U, -1 when solving for V and 0 when solving for W. $\vec{\boldsymbol{U}}_{geo} = (U_{geo}, V_{geo})$ is the geostrophic wind vector, g is the gravitational acceleration constant and θ and θ_0 are the values of the potential temperature and reference potential temperature respectively. Furthermore in equation (2.4), the terms with π and τ are taking into account the calculations of the subgrid filter. $\pi = \frac{p-p_{hyd}}{\rho_0} + \frac{2}{3}e$ is a modified 'pressure' with p_{hyd} the slab-mean hydrostatic pressure, ρ_0 the reference value of the density and e the subfilter-scale turbulent kinetic energy (SFS-TKE). τ is the subgrid momentum flux. In the atmospheric boundary layer, the turbulent eddies differ between the order of millimeters and the order of kilometers. A disadvantage of calculations with LES models is that there is a demand of large computation power. As a solution, a subfilter-scale model is applied on the governing equations in which the turbulent eddies larger than the filter width, which contain the most energy, will be resolved, but the smaller and less energetic eddies are parameterized. This is a neat solution to reduce the cost of computational calculations without ignoring calculations on certain length scales. For a detailed description of the subfilter-scale model and a derivation of the governing equations in DALES, we refer to Heus et al (2010).

2.2. WIND TURBINE IMPLEMENTATION

The wind turbine implementation in DALES was performed by former TU Delft master student, P.A. van Dorp, who verified and validated his parameterization model against power curves of two types of wind turbines and wind farm production data (van Dorp, 2016). In his research, the DALES model was used to study the effect of wind turbines on wake dynamics which showed good agreement with LiDAR observations of the wake velocity deficit in warm farms. The wind turbines in his extension to DALES are described by actuator discs existing of airfoil-shaped blades, each exerting non-uniformly distributed lift and drag forces on the natural air flow and extracting power from the kinetic energy of the air. For this research, two Vestas V80 wind turbines will be incorporated in the simulations which have a rotor diameter of 80 meter. A hub height of 80 meter is chosen for these turbines (TheWindPower, 2017). To minimize the effect of the periodic boundary conditions that are applied in DALES in which the flow of air propagating out of the domain at one end is periodically programmed back as boundary conditions at the other end of the domain, the DALES model performs at each time step the calculations on a domain without wind turbines and saves the values of the parameters at the boundaries. These values at the boundaries are then used for the calculations with turbines. In this way, a wake behind the second wind turbine can not influence the first turbine. Further details and explanations about the wind turbine parameterization are available in van Dorp (2016).

2.3. DETAILS OF THE TWO SIMULATIONS

To be able to perform the two simulations, the initial conditions and boundary conditions need to be specified. In table 2.1, the specifications of the domain for the CBL case and the SBL case are shown.

Table 2.1. Specifications of the domain for the two ABL cases in the namoptions input file.

Domain	CBL	SBL
X	10km	2km
Y	3km	0.6km
Z	0.96km	0.4km
Δx	25m	5m
Δy	25m	5m
Δz	7.5m	3.125m
N_x	400	400
N_y	120	120
N_z	128	128

In table 2.1, (X, Y, Z) is the domain size, (N_x, N_y, N_z) is the number of grid points in the domain in each direction and finally $(\Delta x, \Delta y, \Delta z)$ is the distance between the grid points in each spatial direction. The domain for the CBL case is chosen as 10km by 3km by 0.96km, which is much larger than the domain of the SBL case (2km by 0.6km by 0.4km). In the CBL case the turbulent eddies are larger and a larger domain is needed for DALES to calculate their effect on the development of the wind dynamics better in the atmospheric boundary layer. In the SBL case, the turbulent eddies are of a smaller scale. Therefore, a higher spatial resolution in Δx and Δy is demanded, which is chosen to be $\Delta x = 5m$ and $\Delta y = 5m$. In the CBL case it is of course possible to choose such a same Δx and Δy as in the SBL case, but the simulation would then also take 25 times as long, which is not desired in the limited time of this Bsc project. A $\Delta x = 25m$ and $\Delta y = 25m$ would in this case also suffice for good results. Beside the specifications of the domain for the simulations, DALES needs specifications of the wind turbines. In table 2.2 and 2.3, the specifications of the two wind turbines are displayed for the CBL case and the SBL case simulation.

Table 2.2. Specifications of wind turbine 1 and 2 for the CBL case in the windfarmdata.inp input file.

Turbine Data	1	2
X	4000m	4600m
Y	1500m	1500m
Z_{hub}	80m	80m
R	80m	80m
R_{nac}	1.750m	1.750m
$R_{towertop}$	1.935m	1.935m
$R_{towerbase}$	3m	3m
$C_{d,nac}$	0.3	0.3
$C_{d,tower}$	0.4	0.4
U_{cut-in}	5m/s	5m/s
$U_{cut-out}$	20m/s	20m/s

Table 2.3. Specifications of wind turbine 1 and 2 for the SBL case in the windfarmdata.inp input file.

Turbine Data	1	2
X	400m	1000m
Y	300m	300m
Z_{hub}	80m	80m
R	80m	80m
R_{nac}	1.750m	1.750m
$R_{towertop}$	1.935m	1.935m
$R_{towerbase}$	3m	3m
$C_{d,nac}$	0.3	0.3
$C_{d,tower}$	0.4	0.4
U_{cut-in}	5m/s	5m/s
$U_{cut-out}$	20m/s	20m/s

In table 2.2 and 2.3, (X, Y, Z_{hub}) is the location of the center of the turbine rotor. R, R_{nac}, $R_{towertop}$ and $R_{towerbase}$ are the radii of the rotor, nacelle, tower top and tower base respectively. $C_{d,nac}$ and $C_{d,tower}$ are the drag coefficients of the nacelle and the tower respectively, U_{cut-in} is the cut-in wind speed and $U_{cut-out}$ is the cut-out wind speed. The turbines have the same specifications in both simulations, only their locations in the domain are different for the different ABL cases due to the different domain sizes. The turbines are positioned near the center of the x-axis and y-axis and the turbines are placed a distance of 600m apart in the x-direction, which equals 7.5 times the rotor diameter. A significant distance behind the second wind turbine is taken into account in both cases such that the wake evolution over distance can be displayed fully. Further specifications of the wind turbines are displayed in Appendix 2. To examine the effect of turbulence and friction on the development of wind speed and wind orientation, two horizontal momentum equations are describing the evolution of the two horizontal wind speed components, U and V, which read:

$$\frac{dU}{dt} = fV - \frac{1}{\rho}\frac{\partial p}{\partial x} - \frac{\partial F_x}{\partial z} \tag{2.5}$$

$$\frac{dV}{dt} = -fU - \frac{1}{\rho}\frac{\partial p}{\partial y} - \frac{\partial F_y}{\partial z} \tag{2.6}$$

The first term (on the left) in both equations, $\frac{dU}{dt}$ and $\frac{dV}{dt}$, are the acceleration terms of the flowing wind. The first terms on the right hand side, fV and $-fU$ are terms accounting for the coriolis force which originates from Earth's rotation. The second terms on the right hand side are the horizontal pressure gradients and the third and final terms on the right hand side take friction into account.

The Global Energy and Water Cycle Experiment Atmospheric Boundary Layer (GABLS) initiave performed in 2006 an intercomparison of large-eddy simulation models of the stable boundary layer, which showed good results between different LES models (Beare et al., 2006). The SBL case simulation will be specified the same as the GABLS case. However, for the CBL case simulation adjustments have to be made in the specifications. The two ABL simulations will be performed over a period of 9 hours. In both simulations the initial values of the geostrophic wind components, U_{geo} and V_{geo}, are at first prescribed as $U_{geo} = 8m/s$ and $V_{geo} = 0m/s$, constant as a function of height. The geostrophic wind is the wind that would flow if we assume a steady state wind velocity, $\frac{dU}{dt} = \frac{dV}{dt} = 0$, and if we assume that there is no turbulent friction present, thus $\frac{\partial F_x}{\partial z} = \frac{\partial F_y}{\partial z} = 0$. Equations (2.5) and (2.6) will then turn into equation (2.7) and (2.8) respectively.

$$V_{geo} = \frac{1}{f\rho}\frac{\partial p}{\partial x} \tag{2.7}$$

$$U_{geo} = -\frac{1}{f\rho}\frac{\partial p}{\partial y} \tag{2.8}$$

With these assumptions, we can specify that the horizontal pressure gradients in the x and y direction are constant. To specify the different ABL cases for simulation, the surface heat flux or the potential temperature profile over height has to be prescribed. In DALES both methods are possible. To determine which method DALES will use, the switch 'isurf' in the 'namoptions' input file has to be set at 2 for a forced surface potential temperature or has to be set at 4 when a forced surface heat flux is used. For more information about the different switches and options in the 'namoptions' input file, we would refer to the manual by Heus et al (2015). In the SBL case, switch setting 2 is used with the potential temperature defined as a constant value of 265K up to a height of 100m with an overlying inversion strength of $\frac{\partial \theta}{\partial z} = 10K/km$ as displayed in figure 2.1. In order to stimulate turbulence a random potential temperature perturbation of amplitude 0.05K and zero mean was applied on the first few vertical grid points. For a more complete description of the SBL case, one might consult the original paper of the GABLS case (Beare et al., 2006).

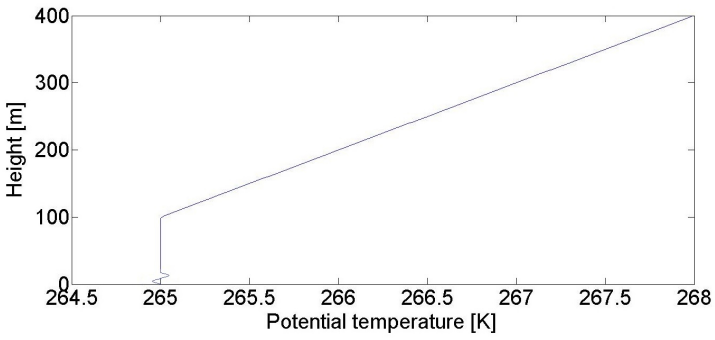

Figure 2.1. Specified potential temperature profile for SBL simulation in the prof.inp input file.

In the CBL case, switch setting 4 is used with the surface heat flux prescribed at a value of 0.05Km/s. Furthermore in the CBL case, a large scale subsidence term of $W_{fls} = -10^{-5} \cdot z$ is imposed on the atmospheric boundary layer to accommodate for the growing atmospheric boundary height due to convection of relatively warm air near the surface of Earth moving upwards. This profile is visible in figure 2.2.

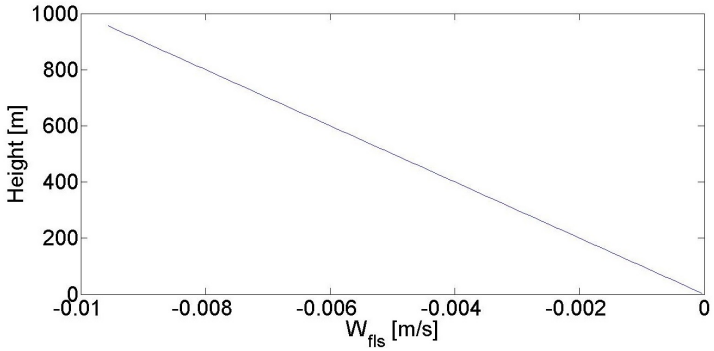

Figure 2.2. Specified large scale subsidence for CBL simulation in the lscale.inp input file.

2.4. ANALYSING DATA

We wish to explore which situation (stable or convective) contains the strongest wake effect on the second turbine and in which situation a higher power yield is achieved. For the examination of the wake profile it is desired that during a period of time the wind is propagating appoximately straight through the wind turbines. In this way, the influence of the wake behind the first turbine on the power production of the second turbine can be visualized. When the output data of a simulation displays that the orientation is at no moment in time in the desired direction, a new simulation is demanded with different specifications of the geostrophic wind or different specifications of the location of the turbines. We have chosen for the first option, however both approaches will achieve the same result. To determine which new geostrophic wind conditions are needed, a possible method is to use equation (2.9) to rotate the wind speed orientation over a certain angle α.

$$\begin{bmatrix} V_{geo,new} \\ U_{geo,new} \end{bmatrix} = \begin{bmatrix} \cos(\alpha) & -\sin(\alpha) \\ \sin(\alpha) & \cos(\alpha) \end{bmatrix} \begin{bmatrix} V_{geo} \\ U_{geo} \end{bmatrix} \tag{2.9}$$

When the new simulation is performed, one can now be sure that the wind orientation is in the desired direction. This method was indeed needed. For the SBL case, the new conditions of the geostrophic wind are $U_{geo,new} = 7.37m/s$ and $V_{geo,new} = -3.12m/s$ and for the CBL case these new conditions are $U_{geo,new} = 7.05m/s$ and $V_{geo,new} = -3.79m/s$. Of course, there are more possibilities for $U_{geo,new}$ and $V_{geo,new}$ which would result in a wind orientation right through the wind turbine configuration at other periods in time, but these values are chosen to achieve the needed wind orientation at the same moment in time for both cases. In figure 2.3 and 2.4 below, a time series of the wind speed orientation at hub height is shown in terms of the east-west component of the wind speed U and the north-south component of the wind speed V for the SBL case and the CBL case respectively.

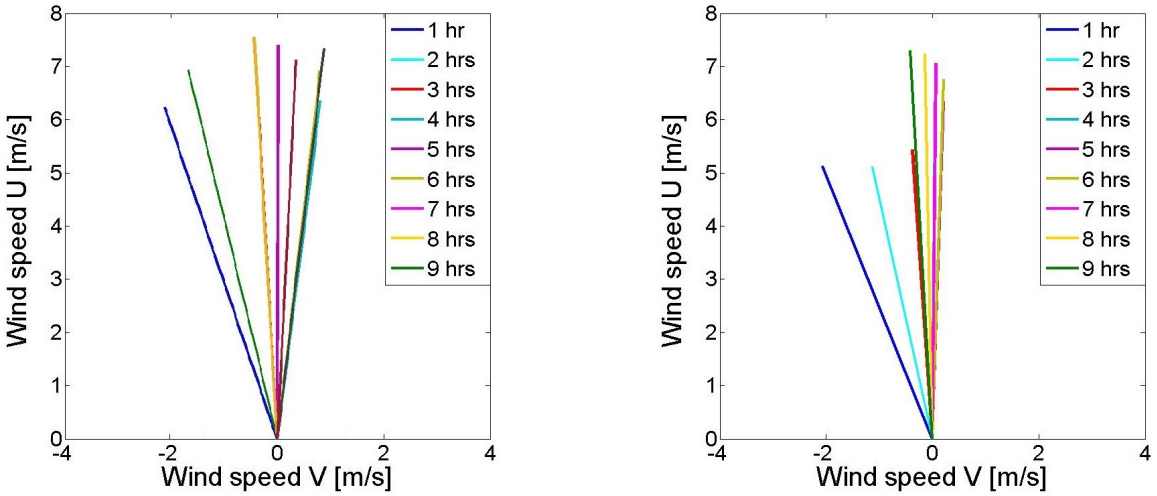

Figure 2.3 and 2.4. Time series of wind speed orientation at hub height of SBL (left) and CBL (right).

From these two figures it can be concluded that indeed during the 9 hours simulation time the wind is propagating a period of time through the wind turbine configuration as the two wind turbines are placed straight in the east-west direction, which corresponds to the wind speed component U. This occurs after around 7 hours for both the SBL case and the CBL case.

All results will be examined with the use of Matlab. Most output data of DALES is displayed in text files in a time series with steps of 10 minutes. To be able to get proper arrays of data out of these text files, a recommendation is to use the option 'Import data' in Matlab and to choose the further option 'Exclude rows with unimportant cells'. After that, a for-loop can be used to place the different steps in time as seperate collumns instead of one long collumn. In the text files, horizontal averages of certain variables are stored. To find the full data in the (x, y, z, t) directions, the netcdf fielddump files need to be examined.

3

WAKE PROFILE EVOLUTION FOR TWO ABL CASES

In this chapter, the simulations of the two ABL cases will be verified and the output data of the simulations will be displayed and examined to find an answer on the optimal ABL case in terms of the power production of this specific wind turbine configuration.

3.1. TURBULENT KINETIC ENERGY PROFILES

Before analysing and comparing the output data of the two simulations, the simulations will be verified on the turbulent kinetic energy (TKE) profiles. In the SBL case, a cool surface layer and relatively little turbulence in the air are present. In the CBL case however, a relatively warm surface layer and high turbulence level are present. These characteristics of turbulence are what we would like to see in the output data of DALES to make sure that the simulations are executed well and that it is acceptable that the results of these simulations are compared and conclusions are extracted out of these results. The total TKE can be divided into a resolved TKE part and a part from the subfilter-scale model. To calculate the total TKE profiles of the two cases, equation (3.1) reads (Heus et al., 2010):

$$TKE = \frac{1}{2}(\overline{u'u'} + \overline{v'v'} + \overline{w'w'}) + \overline{e} \tag{3.1}$$

$\overline{u'u'}$, $\overline{v'v'}$ and $\overline{w'w'}$ are the momentum fluxes of the three wind speed components and $\overline{e}$ is the subfilter-scale turbulent kinetic energy (SFS-TKE) (The overline is used for the spatial-average). For both simulations, DALES calculates the momentum flux of the wind speed components and the SFS-TKE, spatial-averaged over each horizontal slab of the domain at each time step in the 'profiles' output netcdf file. For comparison of the two simulations, the total TKE profile of both cases are placed together in figure 3.1, averaged over a period of one hour between 6.5 and 7.5 hours into the simulation in which period the wind is directed in line with the two turbines. The red line corresponds to the SBL case and the blue line corresponds to the CBL case.

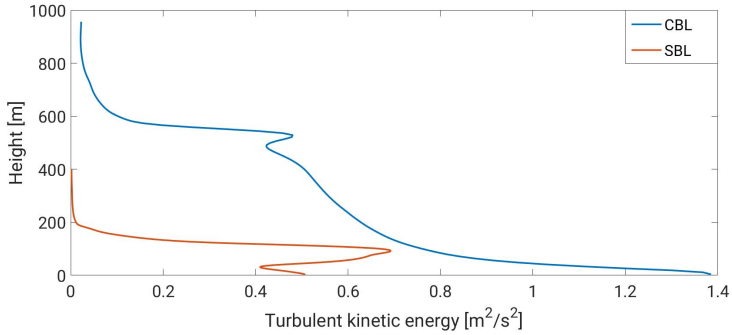

Figure 3.1. Total turbulent kinetic energy profile over height for the two ABL cases, averaged over a period of one hour between 6.5 and 7.5 hours into the simulation.

In the image above, it is clearly visible that the time-averaged total TKE over the domain is considerably larger for the convective case (CBL) than for the stable case (SBL). This is exactly as was expected, because in the CBL case a relatively high turbulence level is present. Therefore, the simulations are now verified in terms of the turbulence characteristics of the two cases which are important for the results of the wind field dynamics.

3.2. WIND SPEED PROFILES

After confirmation that the wind at hub height in both cases will propagate through the wind turbine configuration in some period in time, as shown in figure 2.3 and 2.4, it is now time to look at the wind speed profile over height and over time. In figure 3.2 and 3.3 below, a time series of the wind speed profile over height at each hour of simulation is shown for the SBL case and the CBL case during the 9 hour simulation time. Also in these two figures a black horizontal line is plotted at hub height, which is located at 80 meters.

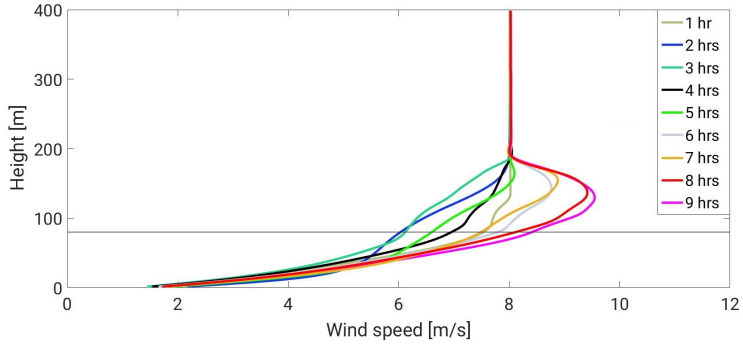

Figure 3.2. Time series of wind speed as a function of height, SBL case.

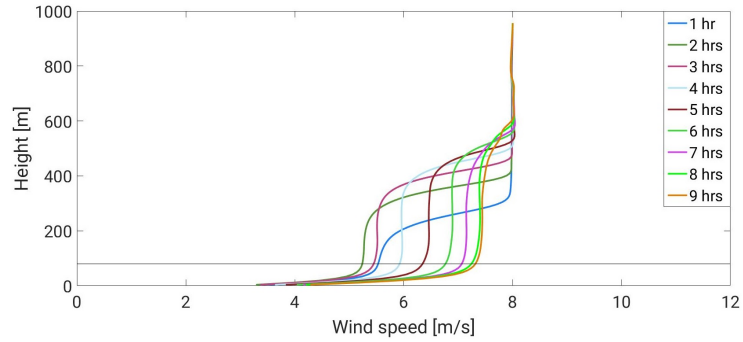

Figure 3.3. Time series of wind speed as a function of height, CBL case.

In both time series, the wind speed profiles at hub height seem to be changing quite a bit over the 9 hours of simulation. Nevertheless, from the two time series it is visible that at each displayed hour of simulation the average wind speed magnitude at hub height in the stable case is slightly larger than in the convective case. This conclusion agrees with meteorological data measurements from the weather station in Cabauw of the Dutch meteorological weather institute KNMI, in which is shown that during nighttime, which corresponds to the SBL case, the average wind speed is higher than during daytime, which corresponds to the CBL case (KNMI, 2017). A research by the Lawrence Livermore National Laboratory shows the same conclusion (Wharton and Lundquist, 2012). Beside only reviewing the wind speed at hub height, the full wind speed profiles of figure 3.2 and 3.3 over height show characteristics of the two ABL cases. In the SBL case wind speed profile in figure 3.2, there is a peak in wind speed visible between a height of 100 meters and 200 meters. Above 200 meters the wind speed stays at a constant value of 8m/s, which equals the magnitude of the geostrophic wind. In the CBL case wind speed profile in figure 3.3, a constant wind speed is shown from 100 meters to around 500 meters high. These wind speed profiles are the result of the total vertical and horizontal momentum fluxes and total TKE profile of both cases. Therefore, to examine the characteristics of the wind speed profiles, figures 3.4-3.8 show the profiles of the total vertical momentum fluxes $\overline{u`w`}$, $\overline{v`w`}$ and $\overline{w`w`}$ and the total horizontal momentum fluxes $\overline{u`u`}$ and $\overline{v`v`}$, as a function of height for the two cases time-averaged over a period of one hour between 6.5 and 7.5 hours into the simulation in which period the wind is directed in line with the two turbines. These data are retrieved from the 'profiles' netcdf output file from DALES.

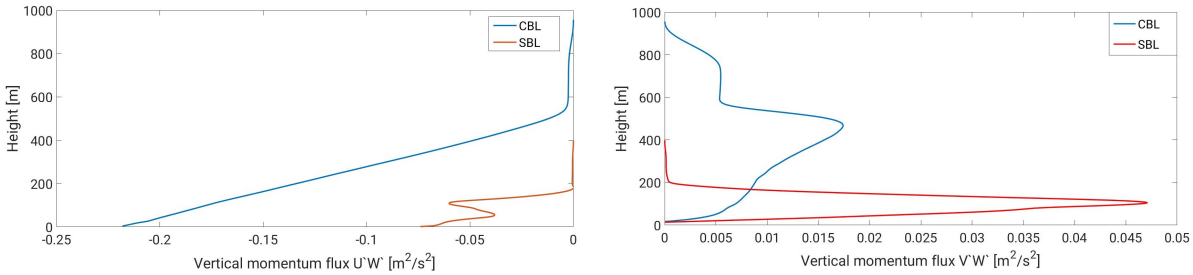

Figure 3.4 and 3.5. Total vertical momentum flux profiles $\overline{u`w`}$ (left) and $\overline{v`w`}$ (right) for the two ABL cases, averaged over a period of one hour between 6.5 and 7.5 hours into the simulation.

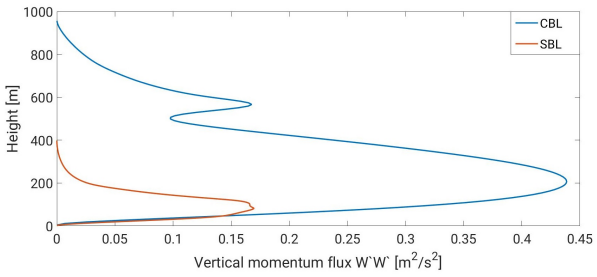

Figure 3.6. Total vertical momentum flux profile $\overline{w`w`}$ for the two ABL cases, averaged over a period of one hour between 6.5 and 7.5 hours into the simulation.

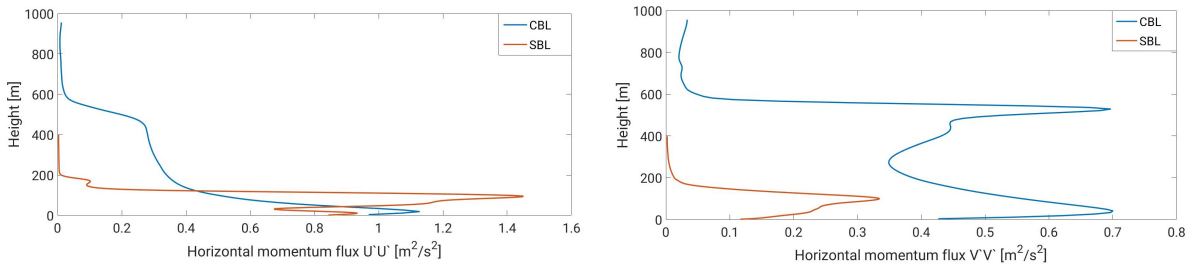

Figure 3.7 and 3.8. Total horizontal momentum flux profiles $\overline{u`u`}$ (left) and $\overline{v`v`}$ (right) for the two ABL cases, averaged over a period of one hour between 6.5 and 7.5 hours into the simulation.

In the atmospheric boundary layer friction with Earth's surface and turbulence, which can also be seen as friction for the wind, make the actual wind speed magnitude differ from the geostrophic wind speed magnitude, the wind speed which is characterized by the absence of friction and turbulence. With increasing height the wind speed is less influenced by friction with Earth's surface and therefore has an increasing trend, approaching the geostrophic wind speed magnitude. Turbulence can be reviewed by the difference between the geostrophic wind speed magnitude and the actual wind speed magnitude and so, the total TKE profile explains the wind speed profile. In the stable case, a peak is visible in all five total momentum flux profiles and the total TKE profile between a height of 100 meters and 200 meters. These peaks are the cause of the trend of the wind speed profile over height to first increase towards the geostrophic wind speed, then to increase beyond the geostrophic wind speed and finally to be pulled back and to approach the geostrophic wind speed, as is displayed in figure 3.2. Above a height of 200 meters, the net total momentum flux and the total TKE equal zero and therefore, the wind speed stays constant at the value of the geostrophic wind speed magnitude above this height.

The momentum fluxes of the convective case show two characteristic peaks in the profiles of $\overline{u`u`}$, $\overline{v`v`}$, $\overline{w`w`}$. A peak is visible between a height of 0 meters and 200 meters and a peak is visible between 500 meters and 600 meters high. The total TKE profile shows these peaks as well. The peaks in the momentum fluxes and the total TKE are the cause of the trend of the wind speed profile over height to first increase relatively quickly towards the geostrophic wind speed up to hub height, which decreases the total TKE. Above hub height, the wind speed increases very slowly, which is the result of a slowly decreasing positive TKE at these heights. Above around 500 meters, the wind speed increases faster towards the geostrophic wind, showing a small peak in the total TKE. Above a height of 600 meters, the total TKE decreases to almost zero at which height the wind speed becomes equal to the geostrophic wind speed.

As a conclusion, for both cases the dynamics in the wind speed profiles over height correspond with the total momentum flux profiles and total TKE profiles.

3.3. WAKE PROFILES

To examine the 3D wind field output data of the simulations, the netcdf fielddump output files of DALES are needed. In figure 3.9 and 3.10 below, instantaneous images of a horizontal slice of the 3D wind field in the (x,y)-plane are plotted at hub height over the whole domain for the two cases, both plotted at 7 hours after the start of the simulation. In both figures, the wind turbines are indicated by black vertical lines. An important remark on these two images is that the x-axis and y-axis sizes are different, because of the different domain sizes for the two cases.

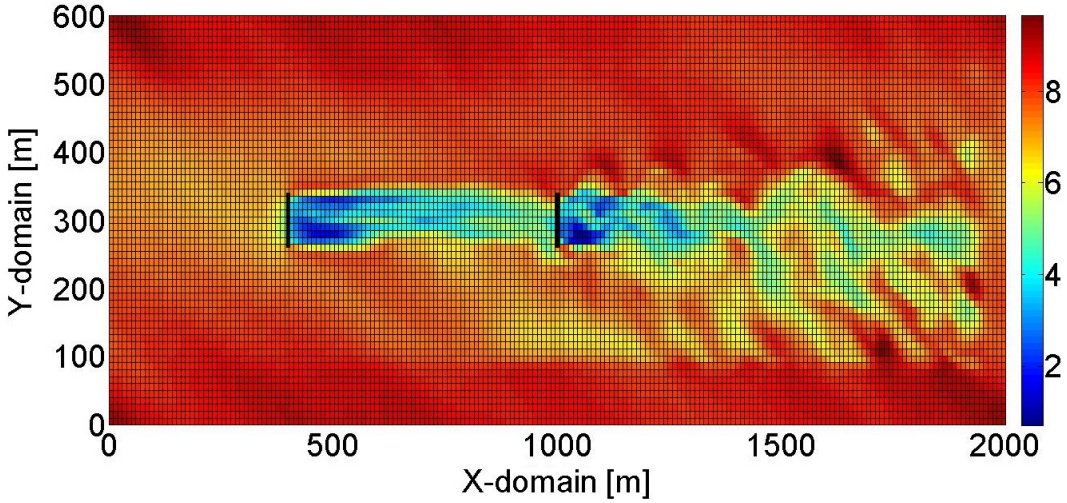

Figure 3.9. Instantaneous image of wind speed field in (x,y)-plane of the domain at hub height and t = 7hrs, SBL case.

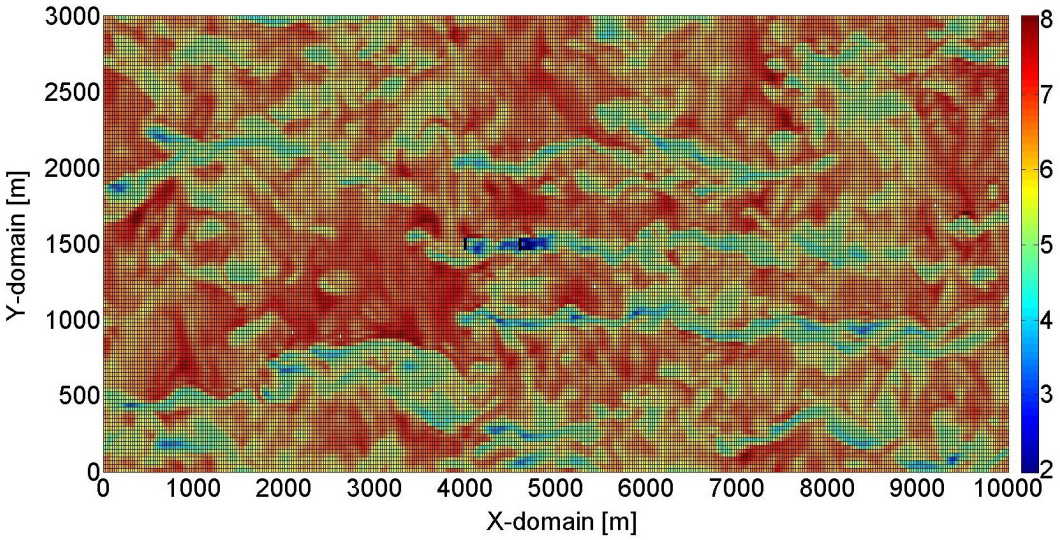

Figure 3.10. Instantaneous image of wind speed field in (x,y)-plane of the domain at hub height and t = 7hrs, CBL case.

In both images of the wind field, the wake profiles behind the two wind turbines are quite clearly visible, especially for the SBL case. These wake profiles show the negative influence of the wake behind the first turbine on the power production of the second turbine. Figures 3.9 and 3.10 also show the difference in turbulence characteristics between the two ABL cases. In the wind field of the SBL case much less turbulence with small scale fluctuations of wind speed is visible in the simulation domain than in the wind field of the CBL case. Unfortunately, the relatively large horizontal grid point distances $\Delta x = \Delta y = 25m$ for the CBL case compared to the SBL case lead to less spatial resolution in figure 3.10. Because of this, the important information about the wake dynamics in the wind turbine configuration is in the convective case not as clearly visible as in the stable case. For a better illustration of the wakes in the CBL case, a small domain around the wind turbines is taken out of the full domain and plotted seperately in figure 3.11.

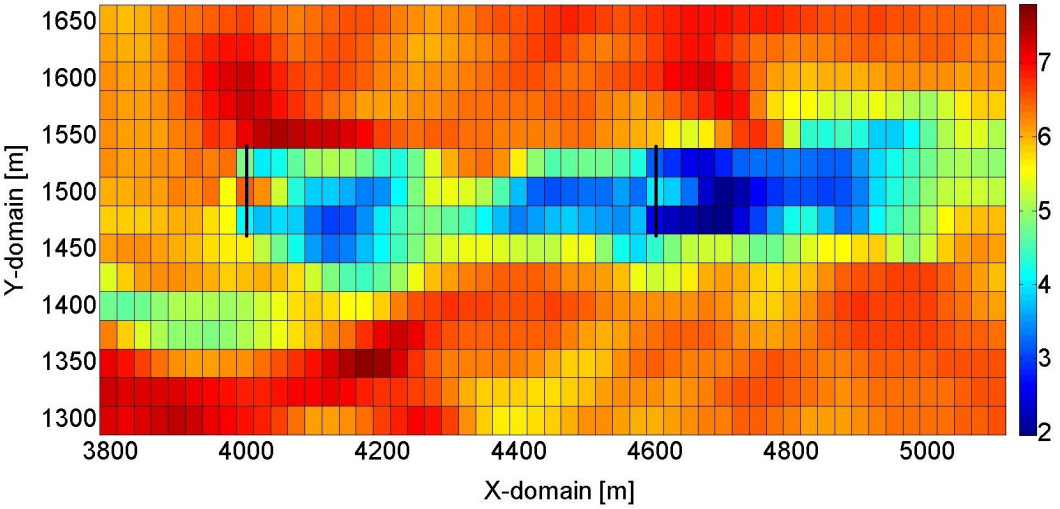

Figure 3.11. Instantaneous image of wind speed field in (x,y)-plane of the domain at hub height and t = 7hrs zoomed in around the wind turbines, CBL case.

Indeed this image gives a better vision of the wakes despite the lower spatial resolution. From the wind field images over the (x,y)-domain it is not clearly visible enough in which case the velocity deficit behind a turbine is the largest and in which case the wakes are the longest. To get more insight in the wake dynamics beside the two horizontal wind fields, in figure 3.12 and 3.13 below two vertical wind fields are plotted in the (x,z)-plane at the center of the y-domain. In figure 3.14 again a small domain is chosen out of the full domain to visualize the wakes better for the CBL case. In all three images again the wind turbines are indicated by black vertical lines.

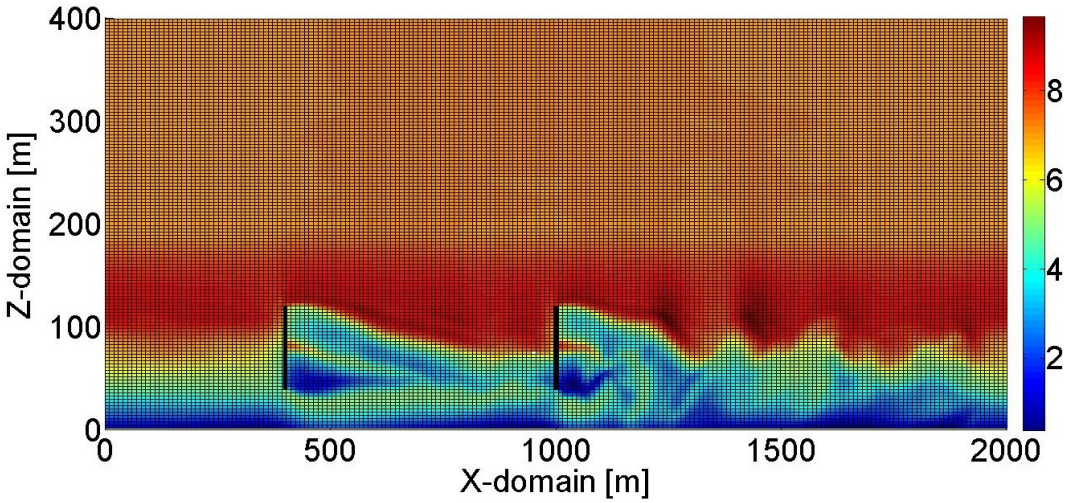

Figure 3.12. Instantaneous image of wind speed field in (x,z)-plane of the domain at y = 300m and t = 7hrs, SBL case.

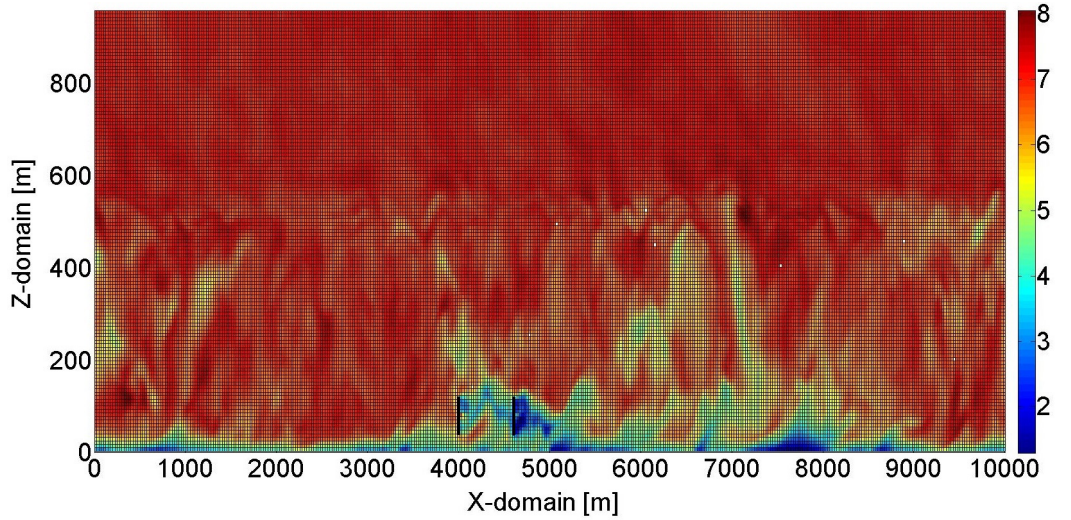

Figure 3.13. Instantaneous image of wind speed field in (x,z)-plane of the domain at y = 1500m and t = 7hrs, CBL case.

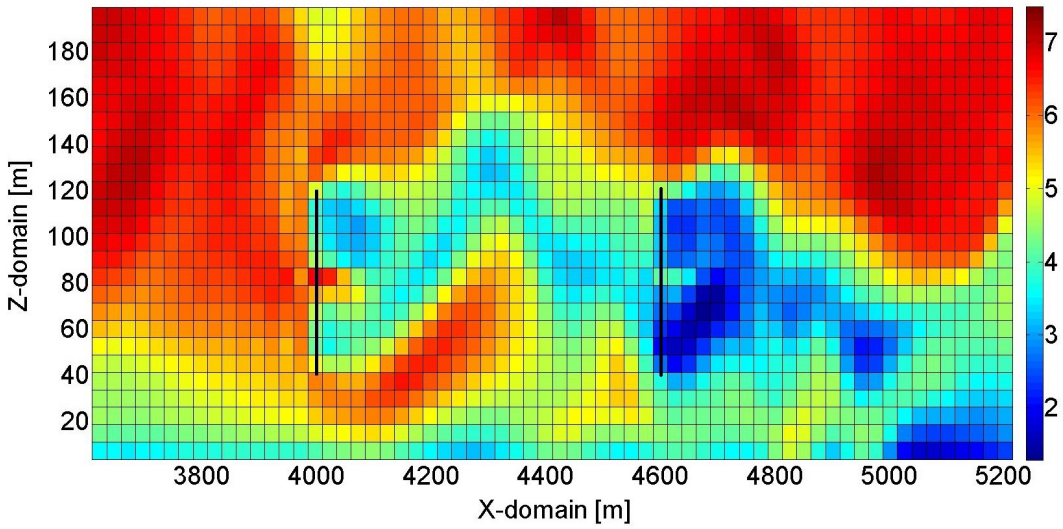

Figure 3.14. Instantaneous image of wind speed field in (x,z)-plane of the domain at y = 1500m and t = 7hrs zoomed in around the wind turbines, CBL case.

Figures 3.12-3.14, make again the wakes behind the turbines clearly visible for both cases. Also, the changes in color over height in the wind speed field of figure 3.12 and 3.13 correspond with the wind speed profiles over height from figure 3.2 and 3.3. For the CBL case, more fluctuations in wind speed are visible in the domain which again correspond with its turbulence characteristic. In the SBL case wind speed field image (3.12) turbulence is much less visible over the domain. At low altitudes in all three images low wind speeds are visible due to friction with Earth's surface. With increasing altitude the effect of friction on wind speed decreases, resulting in a wind speed that approaches the geostrophic wind speed.

From these instantaneous images of the wind field over the (x,y)-plane and the (x,z)-plane, unfortunately no conclusion can be made about in which case the wakes behind the turbines are shorter. A research of former TU Delft bachelor 'Applied physics' student T. Bon shows the observation that the wakes in the CBL case are shorter than in the SBL case (Bon, 2016). The reason for this observation was that in the CBL case there is more turbulent mixing present of undisturbed wind near the wake with disturbed wind in the wake, which will increase the wind speed in the wake faster. However, this can not be concluded from the results of this report.

A proposal for future research on wake dynamics between the SBL case and the CBL case would be to make images of the wind speed field that are not instantaneous at a certain moment in time, but to make images that are averaged over a period in time in which the wind is directed in line with the wind turbines. Another suggestion would be to take the second turbine out of the simulation. In this way the total wake distance can be reviewed fully, instead of a second turbine disturbing the wake recovery of the wake from the first turbine. A combination of the two suggestions above would probably give better results. Unfortunately, these suggestions were not possible to be reviewed in the limited time of this Bsc project. For the research question of this report, it is not necessary to know for which ABL case the wake distance is the shortest. However, for the final conclusion to this report the answer to this question could have been of support to the answer to which ABL case has the optimal power production. Nevertheless, methods to calculate the total power yield will be required to find an answer on the optimal ABL case in terms of power production for this wind turbine configuration.

3.4. POWER YIELD FOR THE TWO CASES

From earlier figures, it is visible that the wake behind the first wind turbine is influencing the power production of the second turbine. In this subchapter, the final calculation of the power yield of the two turbine

configuration will be performed for the two different cases. The approach to calculate the total power yield is to review the wind turbine energy generation output data, calculated and provided by the DALES model. This feature is incorporated in the wind turbine extension to DALES by former TU Delft master student P.A. van Dorp (van Dorp, 2016). The power that the wind turbines extract from the propagating wind is calculated from the torque ξ that is exerted on every grid point within the actuator disk:

$$\xi(x) = r f_i^{wt}(x) \hat{\theta}_i \rho \Delta^3 R^N(x) \tag{3.2}$$

In equation (3.2), $f_i^{wt}(x)$ is the magnitude of the wind force per unit mass and unit area which is multiplied with the fraction of the wind turbine rotor area that is located on grid point x, $R^N(x)$. The tangential component is calculated by multiplication with $\hat{\theta}_i$, the unit vector in the tangential direction. After multiplication with the density of air ρ, the spatial grid distance Δ and the radial distance of a grid point to the hub r, we finally arrive at the torque ξ. The total extracted power P can then be obtained by summation of the torque over all grid points within the actuator disk, multiplied by the rotational speed Ω of the wind turbine:

$$P = \Omega \sum_x \xi(x) \tag{3.3}$$

DALES nicely provides text files with the generated energy per turbine at certain time steps. In figures 3.15 and 3.16, the seperate energy generation profiles for turbine 1 and 2 respectively are shown. In both figures, two black vertical lines are plotted at 6.5 hours and 7.5 hours, which mark the period in which the wind is directed in line with the two wind turbines.

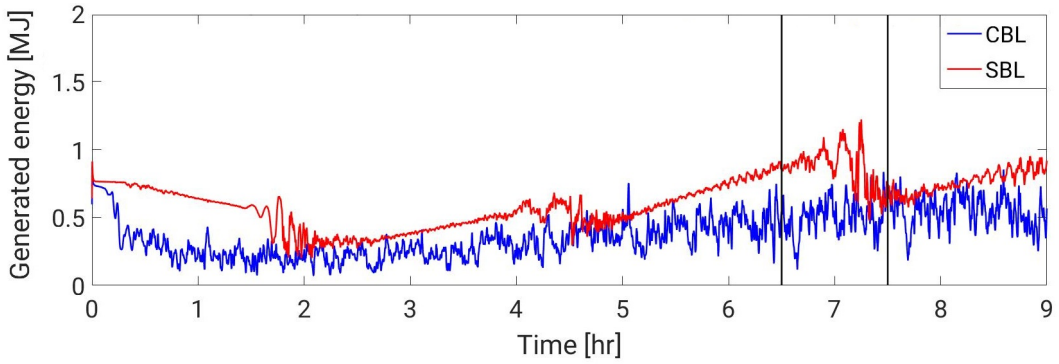

Figure 3.15. Generated energy of turbine 1 over the 9 hours of simulation.

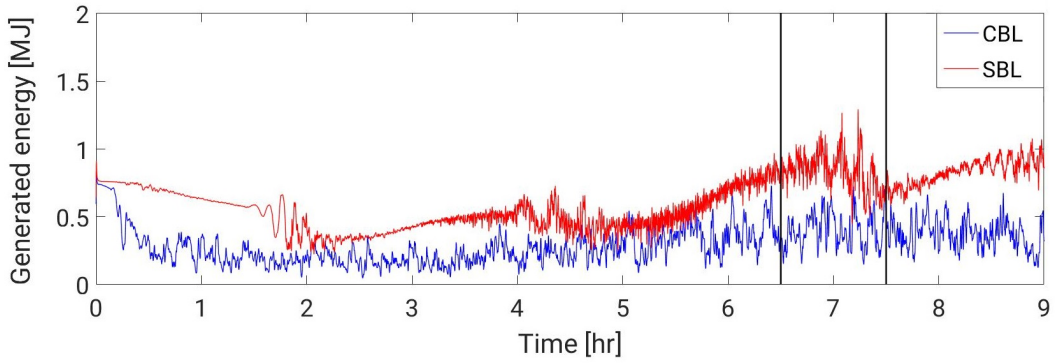

Figure 3.16. Generated energy of turbine 2 over the 9 hours of simulation.

After adding the generated energy profiles of the two turbines together at each time step the total profile can be displayed. In figure 3.17, this energy generation profile is for both cases shown over the 9 hours simulation time.

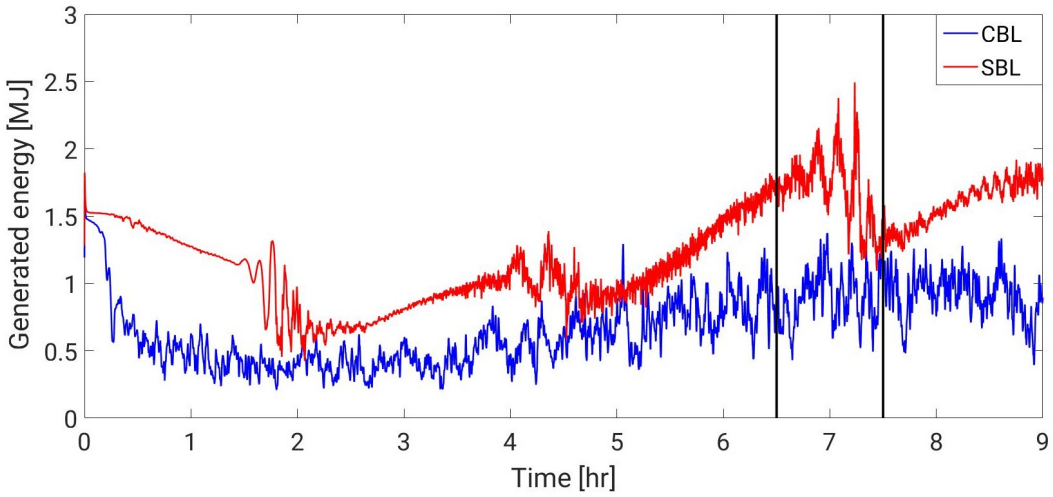

Figure 3.17. Total generated energy of the turbine configuration over the 9 hours of simulation.

The three images above illustrate that the generated energy of a wind turbine configuration can fluctuate significantly over time. The power production of the second turbine is shown to be lower than the first turbine, as was expected due to lower wind speeds at the second turbine. The starting point of the power production of these images is probably the power production that would be the result of the geostrophic wind speed magnitude of 8m/s as this was the initialized wind speed. For the SBL case there are over time periods with small fluctuations in the power production and periods with large fluctuations. It is not exactly known why these characteristics occur in the three figures, but it could be due to the difference in turbulence level over time which lead to fluctuations in wind speed. The power production trend over time is also influenced by the direction of the wind. If the wind is not propagating in line with the two turbines, the frontal area of the rotor that the wind reaches is smaller than the actual area of the rotor, decreasing the power production. Fortunately, we know in which period the wind is directed in line with the two turbines and with this data the total power yield of the CBL case and the SBL case can be calculated using equation (3.4).

$$P_{total} = \frac{\Sigma(E_{turbine,1}(t) + E_{turbine,2}(t))}{T_{period}} \tag{3.4}$$

To perform a fair calculation, the period over which the power yield is averaged is in both cases chosen to be the period of 1 hour between 6.5 and 7.5 hours of simulation time in which the wind is propagating straight through the wind turbines. For the stable case, the total average power yield amounts to $P_{total,SBL} = 1.71MW$ and for the convective case, this amounts to $P_{total,CBL} = 0.90MW$. This rather large difference in power production between the two cases will probably be the result of the higher average wind speed at hub height for the SBL case compared to the CBL case, as shown in figures 3.2 and 3.3. The power production is proportional to the wind speed cubed, as shown in equation 1.1, and this could be the cause of this large difference. Also, from earlier figures 3.9-3.14 the wakes in the full wind speed field showed little difference between the two ABL cases. Altogether, these results conclude that the SBL case is the optimal ABL case in terms of power production for this specific wind turbine configuration.

4

CONCLUSIONS

4.1. CONCLUSIONS

The objective of this thesis was: "Analysing and comparing the wind field and wake evolution in a domain with two wind turbines for two cases, CBL and SBL, to make a conclusion about the optimal atmospheric boundary layer case in terms of the total power yield in a configuration of two wind turbines with the second turbine fully in the wake produced by the one in front, an arbitrary distance of 600m apart." The Dutch Atmospheric Large Eddy Simulation (DALES) model was used to perform the simulations and for each ABL case one simulation was performed. The output data have been analysed with the computer program Matlab to make the illustrative images and to perform the power yield calculations.

Before the start of the simulations, the initial conditions and boundary conditions were prescribed. The simulations have first been validated by reviewing the turbulence characteristics of the two cases through the total TKE profiles and the total horizontal and vertical momentum flux profiles. It was visible that in the CBL case a higher turbulence level was present compared to the SBL case. Also, the dynamics in the wind speed profiles over height corresponded with the total TKE and momentum flux profiles. These wind speed profiles showed that the average wind speed at hub height is slightly larger for the SBL case than for the CBL case. This is in accordance with data from the KNMI weather station in Cabauw, which conclude that the average wind speed magnitude during nighttime (SBL case) is higher than during daytime (CBL case) and is probably due to a lower turbulence level which acts as friction on the propagating wind. Next, the 3D wind fields over the domain have been analysed. From the instantaneous wake profile images over the domain, it was unfortunately not possible to make a conclusion about in which of the two ABL cases the shortest wake is present. Finally, the total power yield of the two turbines has been calculated by reviewing the DALES output data of the generated energy per turbine over the 9 hours of simulation time. The summation of the power yield of each turbine resulted in the total power yield of the total wind turbine configuration. To perform a fair calculation, the total power yield has been averaged over a period between 6.5 and 7.5 hours into the simulation in which the wind is directed in line with the two wind turbines. This resulted in a total average power yield of $P_{total,SBL} = 1.71MW$ for the SBL case and $P_{total,CBL} = 0.90MW$ for the CBL case. This quite large difference in total average power yield is probably due to the higher average wind speed at hub height in the SBL case and the fact that the power production is proportional to the wind speed cubed.

As a final conclusion to all the results in this report, the research objective can be answered as follows: According to the calculations and the figures in this report, the stable boundary layer case is found to be the optimal atmospheric boundary layer case in terms of the total power yield for the wind turbine configuration of two wind turbines, an arbitrary distance of 600m apart, in comparison with the convective boundary layer case.

4.2. RECOMMENDATIONS FOR FUTURE RESEARCH

As a recommendation for research on wake dynamics in the future, I would suggest that images of the wind field should be made that are not instantaneous at a certain moment in time, but to make images that are averaged over a period in time in which the wind is directed in line with the wind turbines. Another suggestion would be to take the second turbine out of the simulation. In this way the total wake distance can be reviewed fully, instead of a second turbine disturbing the wake recovery of the wake from the first turbine. To make the results even better, the simulation of the CBL case should be performed in a higher spatial resolution, even though it will take a significant amount of time to perform the simulation. This will result in much better images of the wake profile dynamics behind the turbines and a clear conclusion can be made on which ABL case has the shortest wake.

Ideas for further research on the topic of power yield of a wind turbine configuration, could for example be the examination of the power yield of a wind turbine configuration of two turbines with varying distances between the turbines. Also, the amount of turbines behind each other could be varied. Furthermore, cases with different atmospheric stability conditions could be analysed by varying the initial prescribed potential temperature profile or prescribed heat flux.

A

APPENDIX 1: WAKE LOSS FORMULA DERIVATION

As discussed earlier in this report, a wind turbine disturbs the natural flow of air when extracting power from the kinetic energy of the air and because of this, there is a wake profile created behind a turbine. This wake in which wind is propagating at a lower speed is slowly mixing together with undisturbed wind that is propagating near the wake. Therefore, over distance the disturbed wind speed is slowly recovering and increasing velocity towards its undisturbed value, U_∞ or U_{atm}. In figure A.1 below, a schematic illustration of the flow of air through a wind turbine is shown together with the different variables that are important for this derivation, namely: the wind speed U, the pressure p and the area of the cylinder in which the air is propagating A. The following derivation is fully provided by Boeker and van Grondelle (2011).

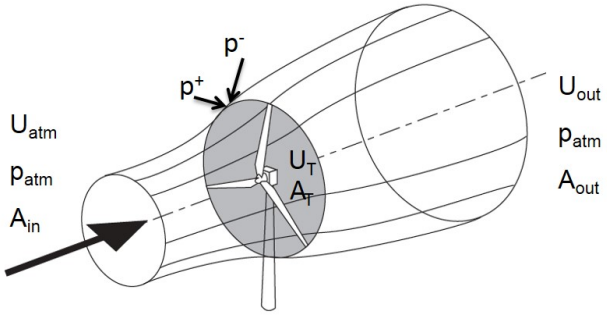

Figure A.1. Schematic illustration of the air flow through a wind turbine (Boeker and van Grondelle, 2011).

At first, a few conservation laws are important. In equations A.1-A.4 the conservation of mass, energy (twice) and momentum are shown respectively. In equation A.5 the power production of an actuator disc is displayed as a formula of the earlier mentioned variables.

$$\frac{\partial M}{\partial t} = \rho A_{in} U_{atm} = \rho A_T U_T = \rho A_{out} U_{out} \tag{A.1}$$

$$\frac{p_{atm}}{\rho} + \frac{1}{2} U_{atm}^2 = \frac{p^+}{\rho} + \frac{1}{2} U_T^2 \tag{A.2}$$

$$\frac{p_{atm}}{\rho} + \frac{1}{2} U_{out}^2 = \frac{p^-}{\rho} + \frac{1}{2} U_T^2 \tag{A.3}$$

$$(p^+ - p^-)A_T = \rho A_{in} U_{atm}(U_{atm} - U_{out}) \tag{A.4}$$

$$P = (p^+ - p^-)A_T U_T \tag{A.5}$$

By substituting the two energy conservation equations, A.2 and A.3, into each other, formula A.6 can be obtained for the pressure difference $\Delta p = p^+ - p^-$ that occurs at the rotor actuator disc. A similar equation for the pressure difference can be found by substituting U_T of the mass conservation formula, A.1, into the equation for momentum conservation, A.5. This result is shown in equation A.7. The two equations for the pressure difference are in equation A.8 combined to obtain a relation between the three different wind speed values U_T, U_{atm} and U_{out}.

$$p^+ - p^- = \frac{1}{2}\rho(U_{atm} - U_{out})(U_{atm} + U_{out}) \tag{A.6}$$

$$p^+ - p^- = \rho U_T(U_{atm} - U_{out}) \tag{A.7}$$

$$U_T = \frac{1}{2}(U_{atm} + U_{out}) \tag{A.8}$$

If we introduce the induction factor a of a rotor as in equation A.9, we see a relation about the loss in wind speed between its undisturbed value U_{atm} and its value just behind the rotor U_T. From this, equation A.10 can be obtained by substitution of equation A.9 into equation A.8.

$$U_T = U_{atm}(1 - a) \tag{A.9}$$

$$U_{out} = U_{atm}(1 - 2a) \tag{A.10}$$

For the wake evolution behind a turbine, first of all a schematic illustration is shown in figure A.2 about the important variables that play a role here. Furthermore, two assumptions are important for the derivation of the wake profile formula. The first assumption is that the wake is conically shaped. This gives rise to equation A.11. The second assumption is that mass is conserved in a cylinder with radius r ($r > r_{out}$), which is displayed in equation A.12.

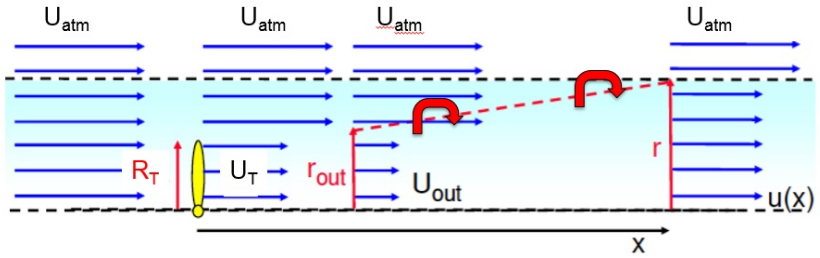

Figure A.2. A schematic illustration of the wake evolution behind a wind turbine (Boeker and van Grondelle, 2011).

$$r - r_{out} = \alpha x \tag{A.11}$$

$$(r^2 - r_{out}^2)U_{atm} + r^2 U_{out} = r^2 U(x) \tag{A.12}$$

To perform the final substitutions and to obtain the final formula for the wind speed evolution in a wake, a few extra equations are needed. The mass conservation in equation A.1 gives a relation between R_T and r_{out} in equation A.13, which can be expressed as only a function of the induction factor a in equation A.14. This equation is rewritten in equation A.15 in which a new variable γ is introduced which is equal to $\gamma = \sqrt{\frac{1-a}{1-2a}}$.

$$U_T \pi R_T^2 = U_{out} \pi r_{out}^2 \tag{A.13}$$

$$(\frac{r_{out}}{R_T})^2 = \frac{U_T}{U_{out}} = \frac{U_{atm}(1-a)}{U_{atm}(1-2a)} = \frac{1-a}{1-2a} \tag{A.14}$$

$$r_{out} = \sqrt{\frac{1-a}{1-2a}} R_T = \gamma R_T \tag{A.15}$$

With the use of equations A.10, A.11, A.12 and A.15 together, the final formula of the wind speed profile in a wake can be determined by following the described assumptions. The result is shown in equation A.16.

$$\frac{U(x)}{U_\infty} = 1 - \frac{2a}{(1 + \frac{\alpha x}{\gamma R_T})^2} \tag{A.16}$$

B

APPENDIX 2: WIND TURBINE INPUT DATA DALES

In this appendix, the characteristics of the Vestas V80 wind turbines will be displayed in more detail. These data are obtained from the master thesis report of P.A. van Dorp (van Dorp, 2016) and are used as input data in DALES. Tables B.1-B.3 show the input data of the pitchrotdata.inp.expnr, liftdragdata.inp.expnr and chordtwistdata.inp.expnr input files.

Table B.1. Blade pitch angle $\beta_{p,0}$ and rotational speed of the rotor Ω as a function of wind speed U_∞, contained in the 'pitchrotdata.inp.expnr' input file.

U_∞ [m/s]	$\beta_{p,0}$ [deg]	Ω [RPM]
5	1.179	12.500
6	0.109	13.240
7	-0.636	14.580
8	-1.000	16.225
9	-1.316	17.400
10	-1.388	18.000
11	-0.161	18.000
12	2.776	18.000
13	6.214	18.000
14	9.325	18.000
15	11.639	18.000
16	13.678	18.000
17	15.612	18.000
18	17.450	18.000
19	18.859	18.000
20	19.159	18.000

Table B.2. Lift and drag coefficients C_L and C_D as a function of angle of attack α, contained in the 'liftdragdata.inp.expnr' input file.

α [deg]	C_L [-]	C_D [-]
-5	-0.170	0.017
-4	-0.099	0.017
-3	0.010	0.016
-2	0.123	0.016
-1	0.232	0.016
0	0.336	0.017
1	0.440	0.017
2	0.546	0.017
3	0.655	0.016
4	0.768	0.016
5	0.864	0.017
6	0.956	0.018
7	1.034	0.019
8	1.112	0.021
9	1.176	0.023
10	1.237	0.026
11	1.275	0.029
12	1.299	0.033
13	1.315	0.038
14	1.309	0.044
15	1.295	0.051
16	1.264	0.075
17	1.224	0.124
18	1.176	0.149
19	1.117	0.171
20	1.068	0.190

Table B.3. Chord length c and twist angle Ω as a function of the radial distance along the rotor blade r, contained in the 'chordtwistdata.inp.expnr' input file.

r [m]	c [m]	β_T [deg]
0	2.406	18.793
1	2.406	18.793
2	2.406	18.793
3	2.406	18.793
4	2.873	17.572
5	3.235	16.391
6	3.415	15.267
7	3.526	14.203
8	3.614	13.141
9	3.595	12.048
10	3.531	10.979
11	3.462	10.085
12	3.363	9.222
13	3.255	8.437
14	3.126	7.663
15	2.995	6.972
16	2.859	6.281
17	2.721	5.638
18	2.562	4.996
19	2.423	4.429
20	2.310	3.922
21	2.194	3.426
22	2.075	2.960
23	1.956	2.493
24	1.851	2.171
25	1.750	1.883
26	1.662	1.602
27	1.584	1.341
28	1.506	1.079
29	1.444	0.852
30	1.385	0.666
31	1.325	0.481
32	1.262	0.328
33	1.198	0.276
34	1.121	0.224
35	1.011	0.158
36	0.900	0.085
37	0.762	0.012
38	0.597	0.002
39	0.317	0.002
40	0.028	0.001

C

ACKNOWLEDGEMENTS

First of all, I would like to thank my personal supervisor Dr. S.R. de Roode for providing the possibility to do my bachelor thesis project at the research group 'Atmospheric physics'. This research group is part of the department 'Geoscience and Remote Sensing' at the faculty of Civil Engineering at the TU Delft. After doing this research project, I can say that I feel content that I was able to expand the knowledge that I gained at the minor 'offshore wind energy' and that I have learned a lot about doing my own research. I learned much about the DALES model, turbulence, atmospheric physics, working in a Linux environment and programming with several kinds of output data. Also, it was the first time for me working with the document preparation system LaTeX. The LaTeX master thesis template of the TU Delft was of great use for the learning process. In the future, I would like to switch from the bachelor education 'Applied physics' to the master 'Applied mathematics', in which I would like to follow the track 'Computational Science and Engineering'. I am sure that I have learned a lot from this research project and that the experience in simulation models and programming can help me in the future with my further education.

Furthermore, I would like to thank my thesis committee, in which not only Dr. S.R. de Roode was present, but also Prof. Dr. A.P. Siebesma. Also, I would like to thank Pim van Dorp for helping me with the wind turbine implementation in DALES and Erwin de Beus for the IT support during my research project. Last but not least, I would like to say a big thank you to my parents for all the support they gave me throughout the years of my bachelor study 'Applied physics'.

D

BIBLIOGRAPHY

Awea, 2016: Reducing greenhouse gas emissions. *American Wind Energy Association.* URL: http://www.awea.org/reducing-greenhouse-gas-emissions.

Beare, R. J., and co-authors, 2006: An intercomparison of large-eddy simulations of the stable boundary layer. *Boundary-Layer Meteorology*, **118 (2)**, 247-272, DOI: 10.1007/s10546-004-2820-6.

Boeker, E. and van Grondelle, R., 2011. Environmental Physics, *Sustainable Energy and Climate Change.* 3rd edition. Wiley-Blackwell.

Bon, T., 2016. Analysis of single wind-turbine wake dynamics with Large Eddy Simulation. *TU Delft Bachelor thesis report.*

Ecotricity, n.d.: Our green energy, the end of fossil fuels. URL: https://www.ecotricity.co.uk/our-green-energy/energy-independence/the-end-of-fossil-fuels.

Elte, 2011: A daily cycle of the planetary boundary layer. *Atmospheric chemistry.* URL: http://elte.prompt.hu/sites/default/files/tananyagok/AtmosphericChemistry/ch10s02.html.

Heus, T. and co-authors, 2010: Formulation of the Dutch Atmospheric Large-Eddy Simulation (DALES) and overview of its applications. *Geoscientific Model Development*, **3 (2)**, 415-444, DOI: 10.5194/gmd-3-415-2010.

Heus, T. and co-authors, 2015: Overview of all namoptions in DALES. *Website Dr. S.R. de Roode.* URL: http://www.srderoode.nl/pubs/Namoptions.pdf

KNMI, 2017: Meteorological wind data of June 2017 from the KNMI database. *Koninklijk Nederlands Meteorologisch Instituut.* URL: http://projects.knmi.nl/klimatologie/daggegevens/selectie.cgi.

Latham, S., 2011: What is the potential of wind energy? *Skeptical Science.* URL: https://skepticalscience.com/What-is-the-Potential-of-Wind-Power.html.

Meyers, J., and C. Meneveau, 2012: Optimal turbine spacing in fully developed wind farm boundary layers. *Wind Energy*, **15 (2)**, 305-317. DOI: 10.1002/we.469.

Multiphysics Cyclopedia, 2017: What are the Navier-Stokes equations? *Comsol.* https://www.comsol.com/multiphysics/navier-stokes-equations.

Piironen, A., 1996: Atmospheric Boundary Layer Structure. *UW Lidar Group*. URL: http://lidar.ssec.wisc.edu/papers/papers.htm

TheWindPower, 2017. Vestas V80 2MW wind turbine specifications. *TheWindPower*. URL: http://www.thewindpower.net/turbine/en/30/vestas/v80-2000.php.

Van Dorp, P.A., 2016: Large-Eddy simulation of wind farms in clear and cloud-topped boundary layers. *TU Delft Master thesis report*.

Wharton, S. and Lundquist, J., 2012. Power generation is blowing in the wind. *Lawrence Livermore National Laboratory*. URL: https://www.llnl.gov/news/powergenerationblowingwind.